Electronic Supplementary Material (ESI) for Nanoscale.

Controlling reaction paths for ultra-fast growth of inorganic nanowires floating in the gas phase - Supporting information -

Richard S. Schäufele,[†,‡] Miguel Vázquez-Pufleau,[†] Afshin Pendashteh,[†] and Juan J. Vilatela[*,†]

†*IMDEA Materials, Madrid, 28049, Spain*

‡*Department of Applied Physics, Universidad Autónoma de Madrid, Cantoblanco, 28049, Madrid, Spain*

E-mail: juanjose.vilatela@imdea.org

Propagation of relevant Raman peaks at varying gas mixture ratios

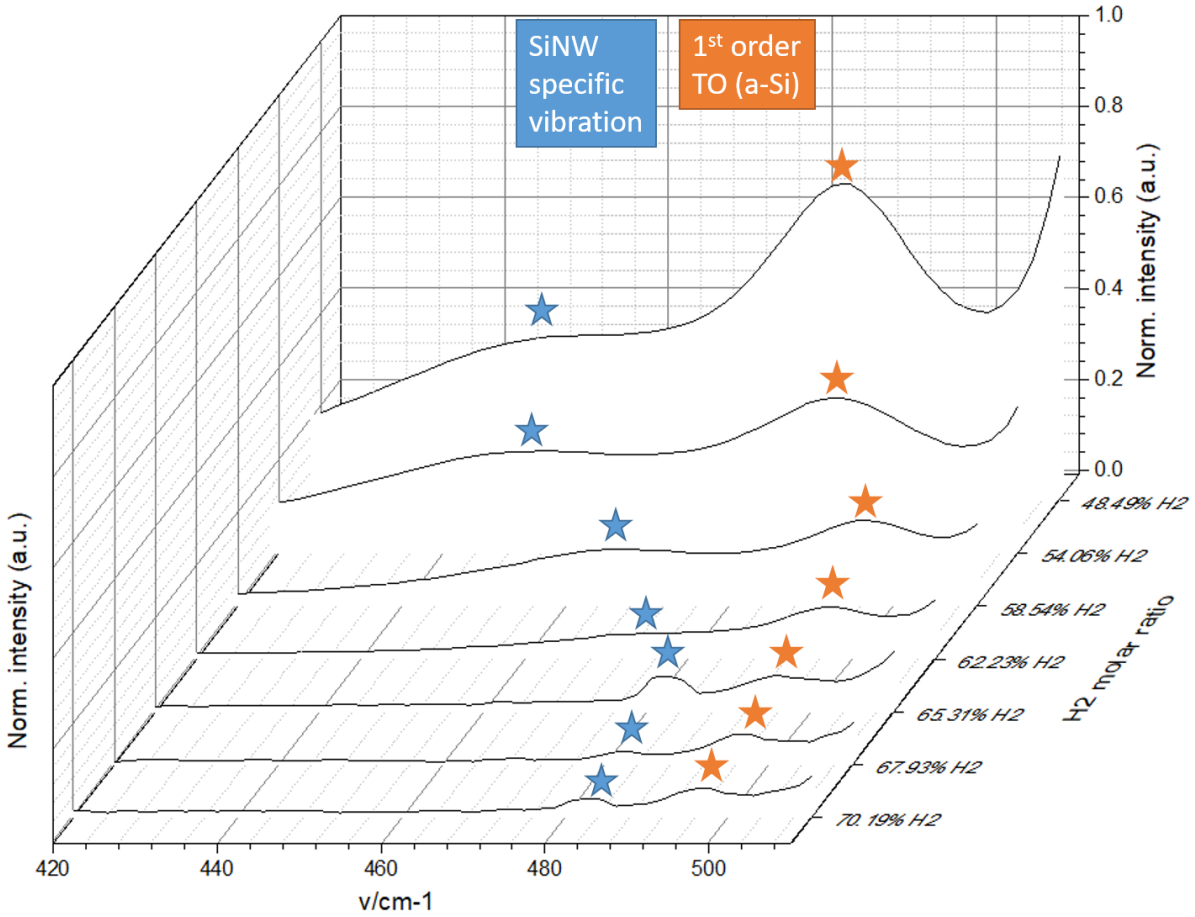

Figure S1: Raman spectra for different SiNW samples showing the decreasing intensity and upshift of the 1st order TO phonon of a-Si with increasing H_2 concentration (orange stars) in the synthesis reaction. Simultaneously, a SiNW specific vibration to the left of the a-Si peak experiences an upshift and a generall decrease in relative intensity as well (blue stars).

Correlation of SiNW contamination and crystallinity studied through SEM.

Raman spectroscopy is extremely suitable for evaluating c-Si and a-Si content of SiNW samples produced at 650°C and 900mbar, as it is highly reproducible and fast as opposed to other methods such as SEM image analysis, where c-Si and a-Si can only be vaguely distinguished via contrast (also depending a lot on image quality), and TEM analysis, which is extremely time consuming and may not represent average distribution. Nontheless, SEM analysis of SiNW samples also support the Raman spectroscopy observations.

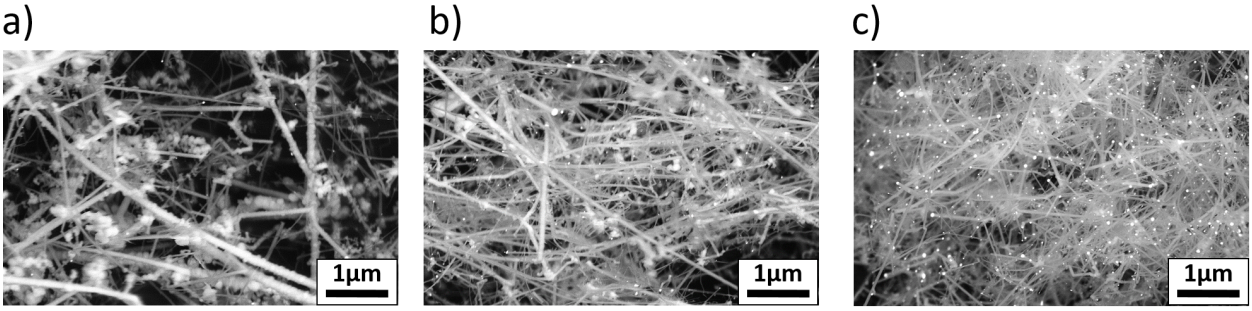

Figure S2: a) SiNWs that correspond to 55% $\bar{C}$. b) SiNWs that correspond to 84% $\bar{C}$. c) SiNWs that correspond to 94% $\bar{C}$.

In Fig. S2 we show SEM micrographs of SiNWs with different $\bar{C}$ (55% $\bar{C}$, 81% $\bar{C}$ and 94% $\bar{C}$). It is clear that the sample with 55% $\bar{C}$ (Figure S2a) contains a larger amount of impurities than the samples with 81 (Figure S2b) and 94% $\bar{C}$ (Figure S2c). While a small amount of impurities can be detected in the sample with 81% $\bar{C}$, impurities cannot be identified anymore in the sample with a respective crystallinity of 94%.

Fig. S2 also demonstrates that SiNWs with low $\bar{C}$ usually feature a larger effective average diameter due to significant radial a-Si loading.

C-Si contamination on SiNWs

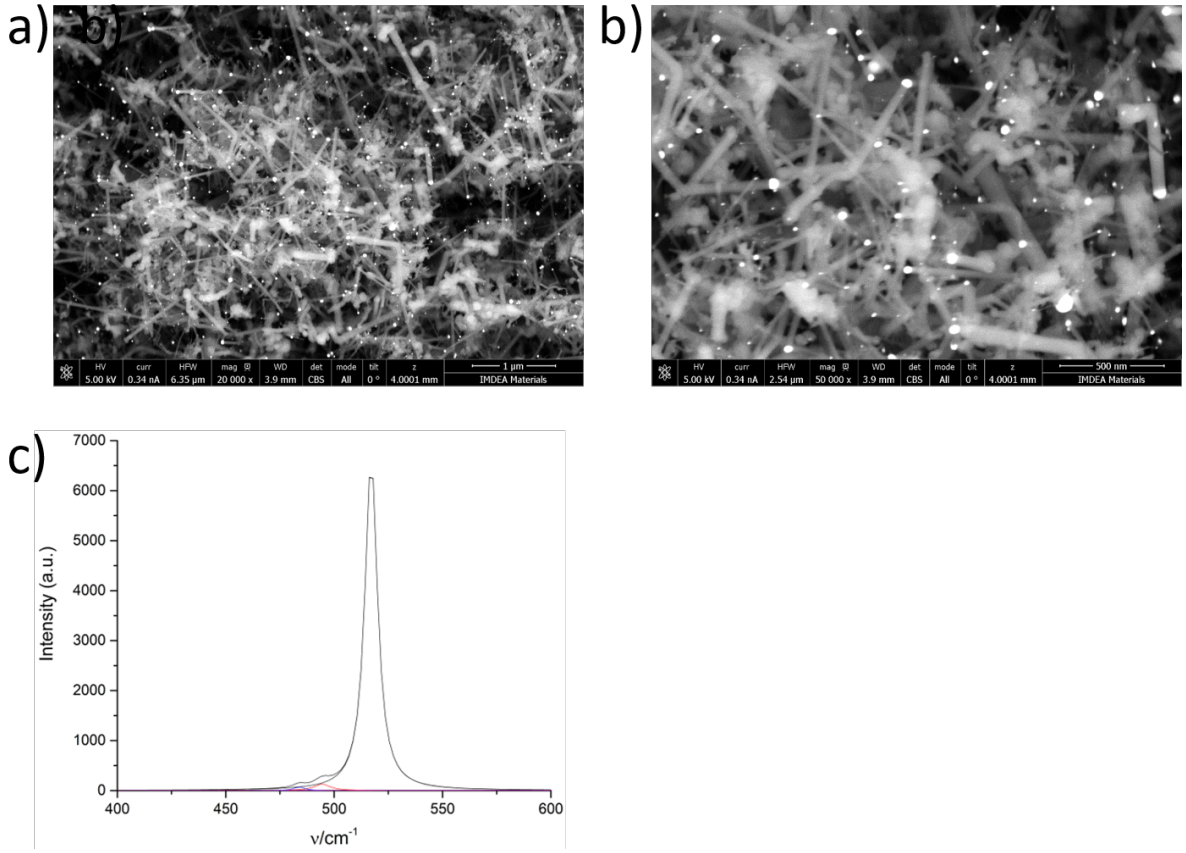

Figure S3: Above 720°C, contamination coming from non-catalised SiH_4 decomposition turns crystalline. Figure a) and b) show SiNWs that have been grown at 750°C. Morphology of the contaminating c-Si seems to be smoother than what is usually observed in a-Si contamination. Fig. c) shows the corresponding Raman spectrum where the intensity of the 1st order TO phonon of a-Si (red curve) is relatively low considering the amount of contamination that can clearly be seen in SEM analysis.

SiNW sample info and mapping of diameter, length, aspect ratio and number concentration

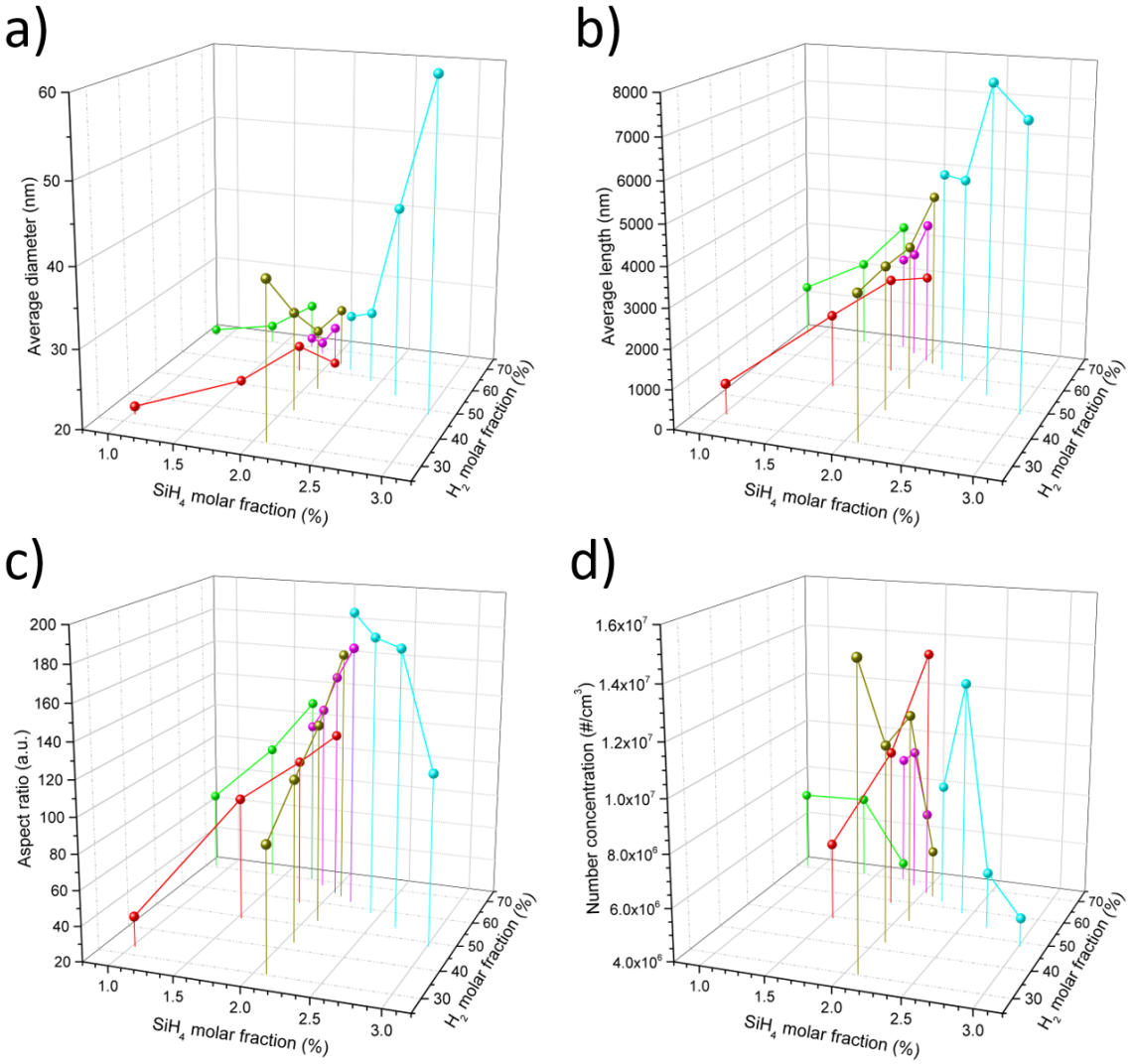

Figure S4: a) Plot of average diameter of SiNWs against H_2 molar fraction and SiH_4 molar fraction for all relevant experiments. b) Plot of average length of SiNWs against H_2 molar fraction and SiH_4 molar fraction for all relevant experiments. c) Plot of average aspect ratio of SiNWs against H_2 molar fraction and SiH_4 molar fraction for all relevant experiments. d) Plot of number concentration of SiNWs during gas phase synthesis against H_2 molar fraction and SiH_4 molar fraction for all relevant experiments.

Figure S5: Experimental details for all relevant experiments

Sample set	Temperature FURNACE [°C]	Time [min]	Pressure [mbara]	Residence time [/30cm]	Molar ratio SiH4 [%]	Molar ratio H2 [%]	Molar ratio N2 [%]
a	650	20	900	5.49	0.8779	70.8015	28.3206
b	650	10	900	5.46	1.3973	70.4305	28.1722
c	650	45	900	5.44	1.7406	70.1853	28.0741
a	650	15	900	9.40	3.0068	48.4966	48.4966
b	650	15	900	8.38	2.6817	54.0657	43.2526
c	650	15	900	7.56	2.4200	58.5480	39.0320
d	650	15	900	6.89	2.2048	62.2333	35.5619
a	650	16	900	6.33	2.0248	65.3168	32.6584
b	650	16	900	5.85	1.8720	67.9348	30.1932
c	650	16	900	5.44	1.7406	70.1853	28.0741
a	650	15	900	12.79	1.0228	32.9924	65.9848
b	650	15	900	9.54	1.5263	49.2368	49.2368
c	650	15	900	7.61	1.8260	58.9044	39.2696
d	650	15	900	6.33	2.0248	65.3168	32.6584
a	650	5	900	6.54	2.0932	30.3849	67.5219
b	650	15	900	6.47	2.0687	42.8762	55.0551
c	650	15	900	6.52	2.0861	52.4899	45.4240
d	650	15	900	6.54	2.0932	64.1458	33.7610

Sample set	Throughput [mg/h]	Effective precursor Conversion [%]	Crystallinity [%]	Avg. Diameter [nm]	Avg diameter STD [nm]	Avg. Aspect ratio [a.u.]	Avg. Aspect ratio STD [a.u.]	Avg. Length [nm]	Avg. Length STD [nm]	Number concentration [#/cm3]
a	3.090	0.062	96.336	20.5	7.2	65.50	16.44	1342.22	460.37	7.06E+06
b	6.080	0.076	97.394	22.2	7.7	99.21	28.03	2204.83	825.28	7.18E+06
c	8.170	0.082	95.283	25.8	9.8	130.28	51.00	3364.27	1441.57	4.66E+06
a	62.570	0.626	55.421	61.4	28.6	117.53	45.46	7211.33	4487.75	5.08E+06
b	47.460	0.475	71.301	44.0	15.1	178.78	43.03	7862.63	3464.46	6.14E+06
c	32.570	0.326	80.901	29.1	11.1	180.60	38.60	5264.25	2255.85	1.30E+07
d	20.830	0.208	90.093	27.3	10.4	191.20	40.50	5216.11	2162.60	8.68E+06
a	10.830	0.108	94.062	24.5	9.0	151.04	53.25	3704.93	1614.99	7.24E+06
b	8.750	0.088	96.571	21.4	5.8	128.83	31.78	2754.71	1103.83	9.54E+06
c	7.820	0.078	96.423	21.2	10.6	116.14	20.61	2466.44	1322.06	9.02E+06
a	0.000*	0.000*	97.414	21.0	8.6	37.21	12.03	781.56	358.02	0.00E+00**
b	2.490	0.050	96.895	20.7	9.3	90.70	12.10	1875.00	886.60	6.95E+06
c	7.500	0.100	97.529	23.3	10.3	105.40	36.70	2456.00	1119.10	1.01E+07
d	8.070	0.081	98.320	19.6	7.9	116.70	27.60	2290.50	1178.00	1.36E+07
a	55.800	0.558	58.572	39.7	16.3	90.77	20.53	3602.05	1615.59	1.51E+07
b	28.800	0.288	79.793	32.4	13.0	112.37	22.92	3645.13	1502.50	1.14E+07
c	22.000	0.220	88.542	27.6	11.0	134.02	23.45	3698.96	1600.09	1.20E+07
d	12.920	0.129	95.212	27.4	10.7	165.33	58.21	4527.77	2559.65	5.84E+06

Values marked with a star symbol (*) could not be measured due to insufficient amount collected. Thus they were set to "0". (**) Without throughput the Number concentration can not be calculated.

The diameter of AuNPs and SiNWs were measured from SEM pictures (image analysis performed with ImageJ) of SiNW samples at a magnification factor of at least x50 000 in order to ensure satisfactory resolution. For each sample, the SiNW diameter was obtained by measuring at least 50 SiNWs. Regarding the given average AuNP diameter for specific samples (see manuscript), at least 50 SiNW gold tips were measured with the exception of highly contaminated samples. In the latter case AuNPs are very difficult to identify as the

majority of AuNPs are covered by Si, which is why a minimum of 20 particles were measured for highly contaminated samples.

The introduced average AuNP diameter, noted in the manuscript's methods part, was determined from SiNW samples with very high Crystallinity (C > 96.0%), in order to ensure that gold nanoparticles with relatively small dimensions were not missed during image analysis. In this, the average AuNP diameter was obtained from 168 AuNP measurements of 3 distinct high crystallinity samples. It is noted that all three samples were produced at evaporation chamber standard conditions (carrier gas type: N_2; carrier gas flow: 2slm; temperature: approx. 1500°C) that were held constant throughout all reported experiments in order to ensure a constant initial AuNP distribution and a constant volumetric number concentration.

With respect to measuring SiNW aspect ratios, the magnification used for the length measurement varied depending on respective SiNW dimensions. In order to obtain average aspect ratios, a minimum of 10 SiNWs per SiNW sample were analyzed on diameter and length via image analysis of SEM images using ImageJ software. It is noted that SiNWs were never exposed to any sonification (or else) to guarantee original SiNW length and morphology, thus, fully intact SiNWs were identified. From our aspect ratio measurements, we also extracted average SiNW length data for each sample (See figure S5).

Catalyst activity

Catalyst activity (in terms of whether or not a catalyst particle catalyzes a nanowire) is assumed to be close to 100% and is not significantly influenced by the gas mix ratio. Our claim is based on the following observations:

1. During all experimental conditions that are reported, AuNPs have not been found on SiNW sidewalls or isolated. Every identified AuNP came with a catalyzed SiNW.

2. The number concentration of SiNWs, meaning the number of SiNWs per cubic centimeter and therefore the number of active catalyst particles, remains surprisingly stable throughout all reported experiments where gas mix ratio is greatly varied. To be more specific, taking into account that 4 independent variables (average SiNW diameter, Average SiNW aspect ratio, collected SiNW sample weight, total gas flow per minute through reactor) must be considered in order to calculate the number concentration of each sample, the **average** number concentration throughout **all** reported experiments turned out to be astoundingly narrow with $8.98\text{x}10^6 \pm 3.04\text{x}10^6$.

3. As supported by Figure S4 d), no clear global trend can be identified with respect to varying gas mix ratios.

FCCVD without hydrogen

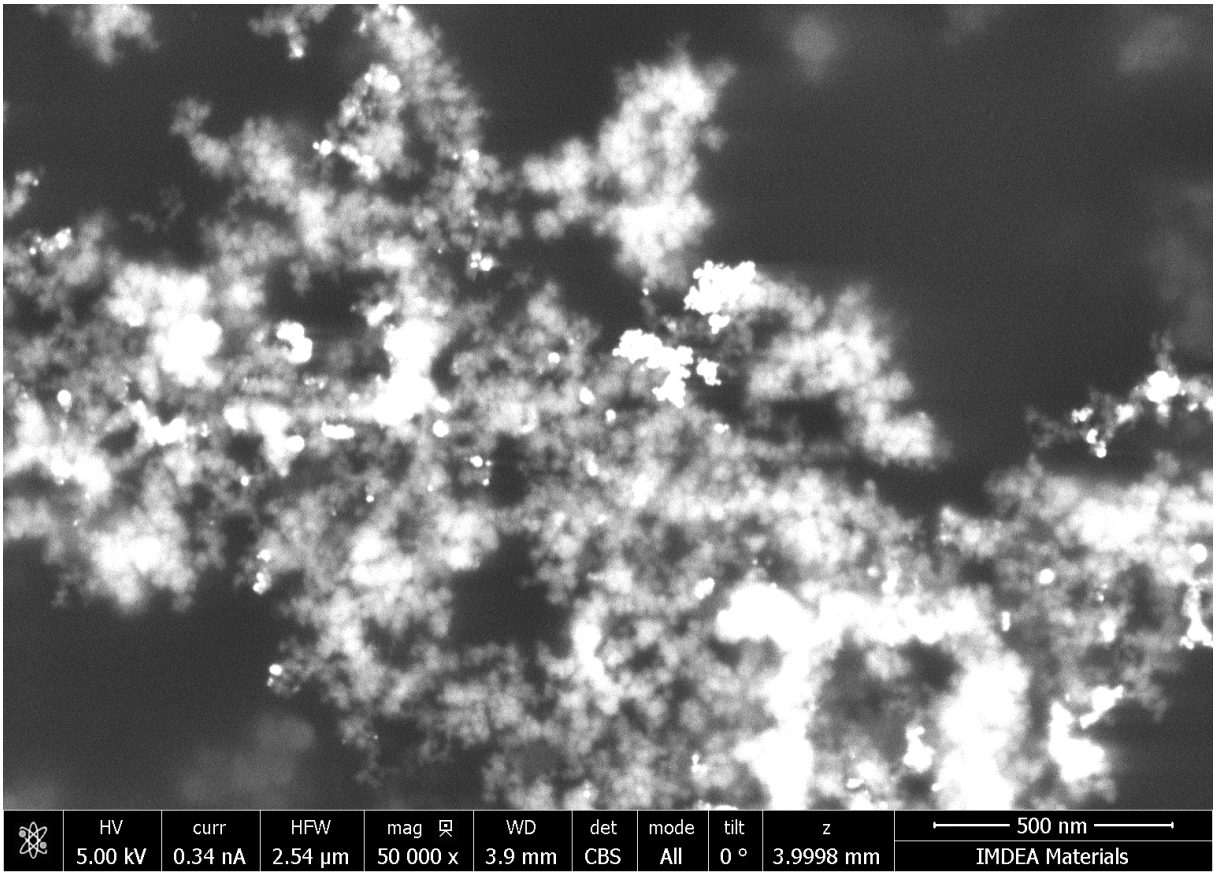

Figure S6: Structures were synthesized at a SiH_4:N_2 ratio of 1:1136 at 650°C, 900mbar and standard AuNP generation (see methods). The vast majority are particles.

Methodology of determining crystallinity

In order to determine Raman-derived crystallinities reflecting mass fraction of the c-Si phase, the procedure outlined in the work of Bustarret et al. was followed.[1] Thus, it is necessary to determine a weighting factor α, that adjusts Raman scattering of the a-Si phase relative to the c-Si phase. By doing this, the respective volume fraction of each phase is obtained. However, since density of a-Si and c-Si differs by less than 2%, the volume fraction is virtually equal to mass fraction. The weighting factor α can be determined by measuring the crystallite size L through WAXS measurements, using the Scherrer equation[2] and applying it to the following equation[1] taken from Bustarret et al.:

$$\alpha(L) = 0.1 + e^{-\frac{L}{250}} \tag{1}$$

Thus, we chose 4 distinct SiNW samples that significantly differ in apparent amount of impurities (see S7b) and perfomed WAXS measurements. The respective XRD patterns (background subtracted and normalized) are presented in Fig. S7a. From these we could extract an average crystallite size of 18.6nm ±2.3nm which resulted in α=0.58.

Additionally, the WAXS profiles shown in Fig. S7a can also be used to determine the degree of crystallinity $\bar{D}$, a qualitative measure of the c-Si ratio. In this, the area of all first order c-Si peaks are summed yielding $Si_{c\_1^{st}}$ and evaluated against scattering intensity of the first order a-Si peak $Si_{a\_1^{st}}$ as follows:

$$\bar{D} = 100 \cdot \left(\frac{Si_{c\_1^{st}}}{Si_{a\_1^{st}} + Si_{c\_1^{st}}}\right) \tag{2}$$

Table S1 lists obtained $\bar{D}$- and $\bar{C}$-values for the four samples and Fig. S7c displays a plot of $\bar{D}$-values against corresponding $\bar{C}$-values. This data can then be fitted resulting in a linear fit curve with a slope of 0.79. Since this value is relatively close to 1, we recognize that $\bar{D}$-values serve as a good estimate for mass fractions of c-Si in mixed phases.

Table S1: Comparison of XRD- and Raman-derived crystallinities for 4 distinct SiNW samples that significantly differ in crystallinity.

	XRD-derived $\bar{C}$ (%)	Raman-derived $\bar{C}$ (%)
Sample A	98.14	96.57
Sample B	87.86	90.09
Sample C	65.79	71.30
Sample D	44.81	55.42

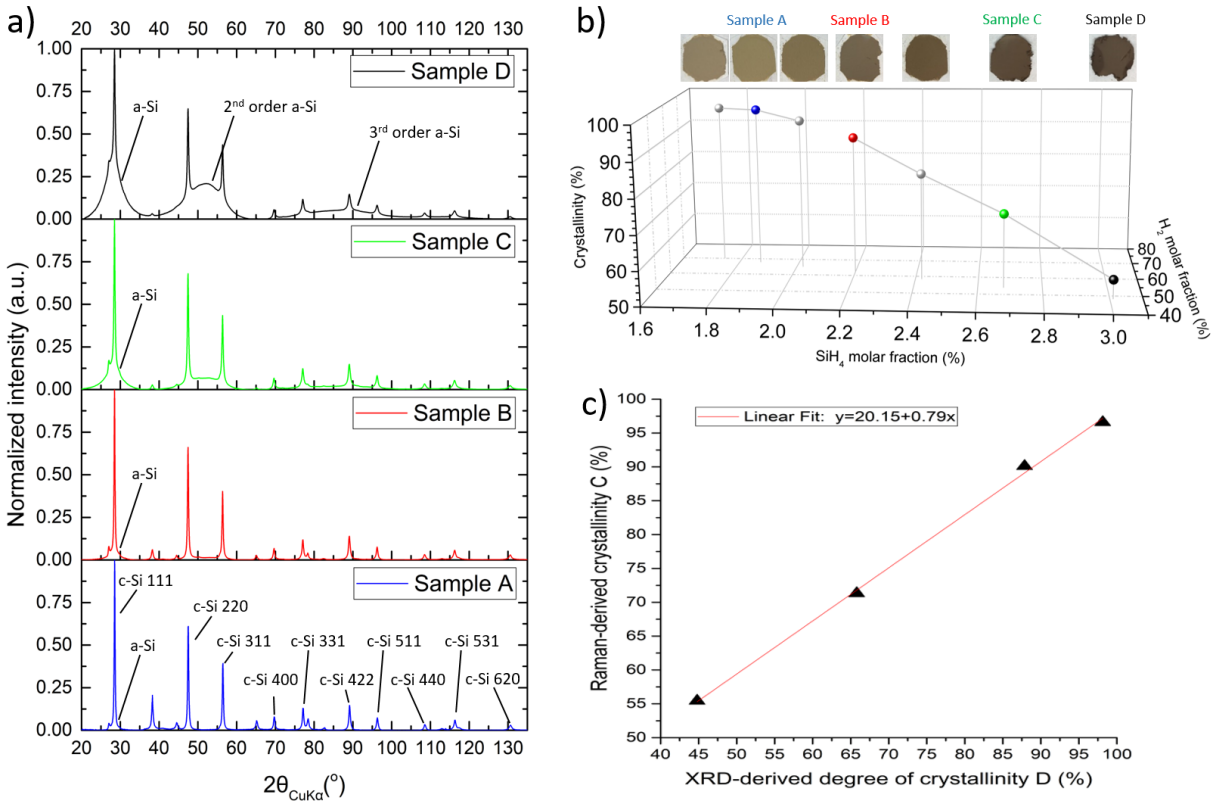

Figure S7: a)Background subtracted and normalized WAXS profiles of 4 different SiNW samples that differ significantly in Raman-derived crystallinity. These four samples are the ones which are colourized black, green, red and blue in figure b). Figure c) shows Raman-derived $\bar{C}$-values and XRD-derived $\bar{D}$-values for the same SiNW samples plotted against each other. This data can be fitted, resulting in a linear fit curve with a slope of 0.79.

Approach to obtain fitting parameters in kinetic model

A supervised algorithm has been implemented to solve equation 5 in the main manuscript based on the independent variables of the experimental data. The results are then compared vs the experimentally determined crystallinity. The difference between predicted and experimental crystallinity squared gives the error squared of a single data point. By summing all of these square errors, a total error square value for a given combination of fitting parameters (η_{FCCVD},$\frac{k_3}{k_2}$, $[SiH_{4sat}]$) can be extracted. By scanning through wide ranges of a single fitting value systematically, a local minimum can be found. The absolute minimum is obtained by employing a supervised methodology that scanns through all 3 fitting parameters iteratively, an approach that is graphically shown in Figure S9.

Mathematically, the minimum squares approach has the following form

$$\mathrm{S} = \sum (\bar{C}_{iexperimental} - \bar{C}_{model})^2 \tag{3}$$

where S is the sum of square error, $\bar{C}_{iexperimental}$ is the experimentally determined crystallinity for i condition, and $\bar{C}_{model}$ is the crystallinity predicted by the model for the same conditions. In the present study, each crystallinity value is a function of the following

$$\bar{C}_{\mathrm{iexperimental}} = \mathrm{f}([SiH_4], [H_2]) \tag{4}$$

$$\bar{C}_{\mathrm{model}} = \mathrm{f}([SiH_4], [H_2], \eta_{FCCVD}, \frac{k_3}{k_2}, [SiH_4]_{sat}) \tag{5}$$

The solution is found when the minimum of the function S is found by systematically scanning through the fitting parameters. η_{FCCVD},$\frac{k_3}{k_2}$, $[SiH_4]_{sat}$ by using a supervised convergence approach as shown in Figure S8

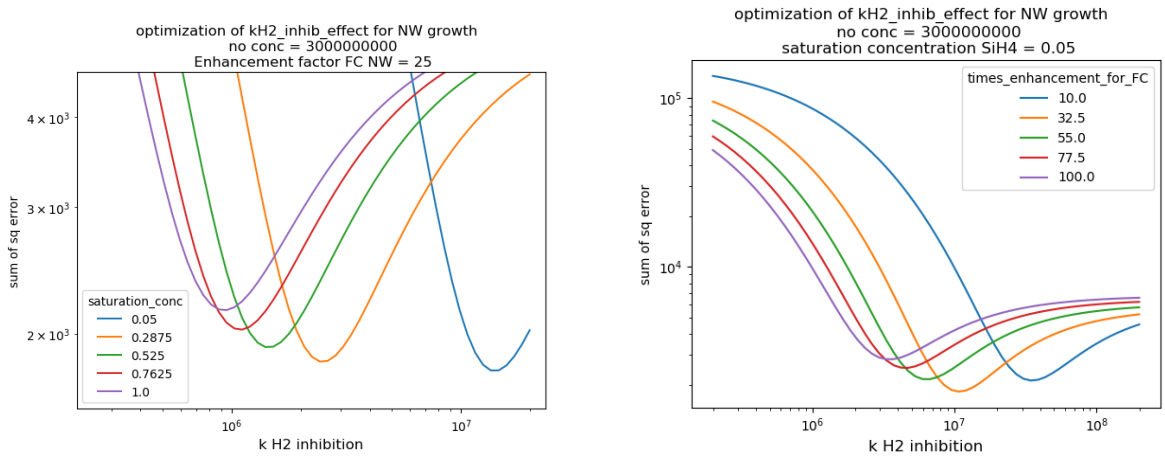

Figure S8: a) Explanatory figure that shows the Summation of square error for different sets of fitting parameters. For a) enhancement factor is kept constant and k H2 inhibition parameters are scanned for different saturation concentrations. For b) saturation concentration is kept constant while k H2 inhibition is scanned through for several times enhancement factors. Convergence is achieved by obtaining the minima in the 2-D plots and then selecting the minima values as the constant parameter for the next iteration. The global minimum is obtained once further optimization iterations do not change the numerical values of the fitting parameters.

Model for estimating total nanowire length

Figure S9 shows the predicted length of the nanowires given the initial conditions of hydrogen and silane concentration. The numerical value is obtained by using the following expression

$$\text{length}_{\text{nw}} = \int_0^{\text{t}} \text{v}_{\text{nw}} \text{dt} \tag{6}$$

where eq. S 6 is solved coupled with eq. 4 from the main manuscript. The total aerosol concentration used to solve this equation is by following assumption d) where wall effects are neglected. By using a mass balance between precursor and produced nanowires, a concentration of around 3 *10^9 is obtained and used for the calculation of Figure S9

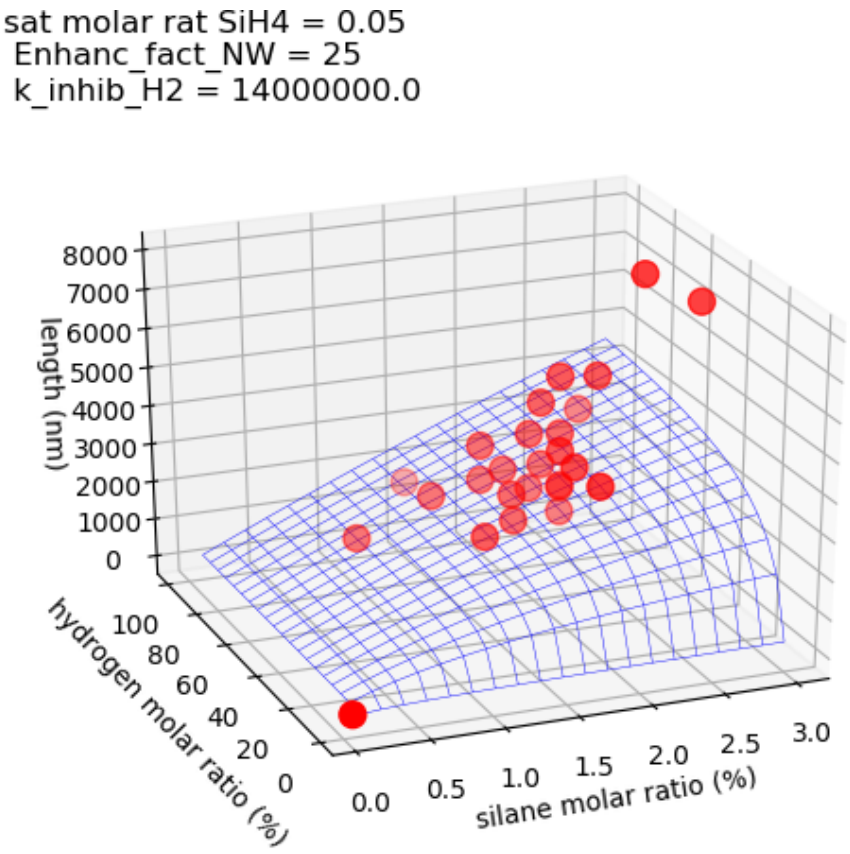

Figure S9: Predicted nanowire length based on the solution of the coupled kinetic model from the main manuscript. The total length is obtained by integrating nanowire growth velocity with respect to time until achieving full conversion in the reaction.

Comparative exercise of two rate processes relevant for NW synthesis

The implications of having a saturation effect means that the velocity of silicon incorporation from silane into silicon nanowires might be slowed down at the catalyst or at the crystallization in the nanowire. Figure S10 shows a preliminary calculation of the velocity of silicon atoms arrival from the gas phase as compared to saturation of silicon in gold, and the reported diffusion of silicon in gold at 650°C, with a diffusion coefficient of about $5.63184 * 10^{-11}\ m^2/s$.[3] Figure S10 shows that collision frequency is a directly correlated with silane concentration. It also shows an estimate of the maximum transport capability of a single gold catalyst nanoparticle. The saturation limit is obtained by the intersection of both the diffusion and the collision frequency functions. An estimation of such saturation point is given in Figure S S10. There, the saturation from transport is considered to be around 6% silane molar ratio. Since the converged value of the saturation concentration obtained via eq S 3 is 0.05% silane. This suggests that diffusion of silicon through the gold catalyst might not be the rate limiting step, in agreement with reports.[4] This leaves crystallization rate and gas to liquid transport as potential responsible to be the rate limiting step in nanowire growth.

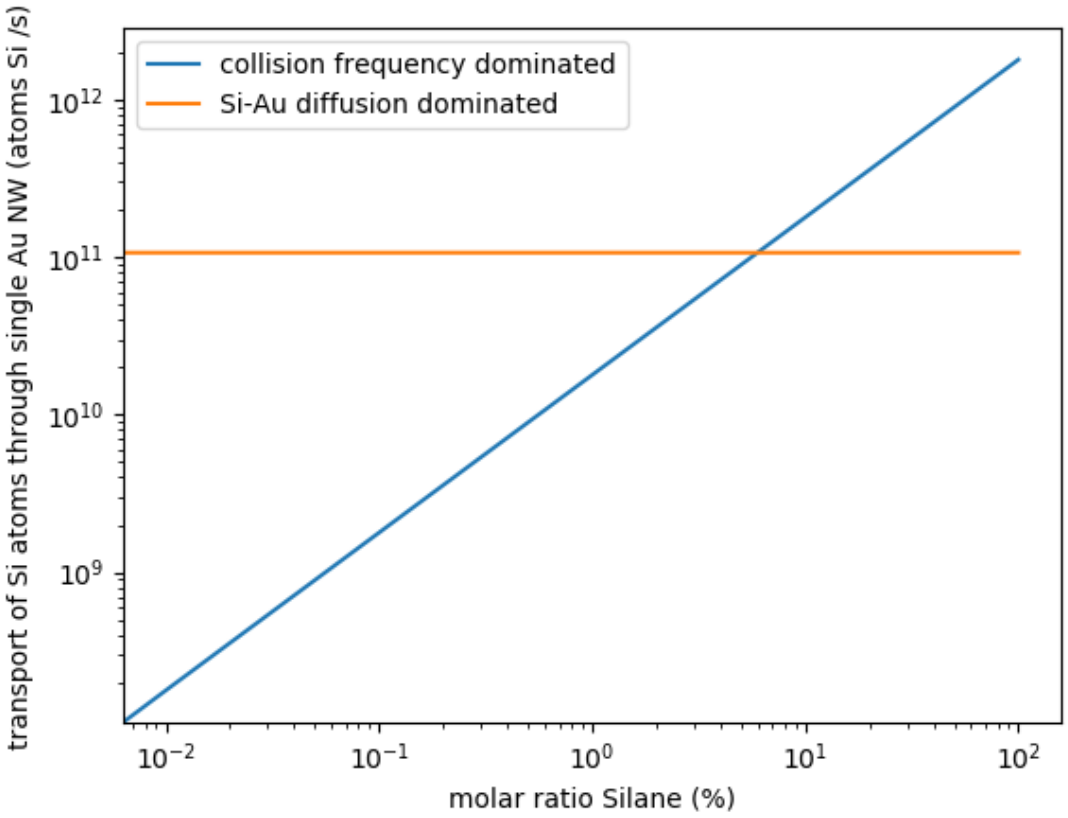

Figure S10: a) Comparison of collision frequency and diffusion capacity for one single nanparticle of gold catalyst. Collision frequency dominates up to about 6% silane molar ratio at the experimental conditions and above this diffusion of silicon through the catalyst dominates

References

(1) Bustarret, E.; Hachicha, M.; Brunel, M. Experimental determination of the nanocrystalline volume fraction in silicon thin films from Raman spectroscopy. *Applied Physics Letters* **1988**, *52*, 1675–1677.

(2) Holzwarth, U.; Gibson, N. The Scherrer equation versus the'Debye-Scherrer equation'. *Nature nanotechnology* **2011**, *6*, 534–534.

(3) Li, Y.; Shi, W.; Gupta, A.; Chopra, N. Morphological evolution of gold nanoparticles on silicon nanowires and their plasmonics. *RSC Advances* **2015**, *5*, 49708–49718.

(4) Lew, K.-K.; Redwing, J. M. Growth characteristics of silicon nanowires synthesized by vapor–liquid–solid growth in nanoporous alumina templates. *Journal of Crystal Growth* **2003**, *254*, 14–22.